Received: 3 August 2022 | Accepted: 27 January 2023

DOI: 10.1111/2041-210X.14089

Methods in Ecology and Evolution

RESEARCH ARTICLE

Body condition changes at sea: Onboard calculation and telemetry of body density in diving animals

Taiki Adachi[1,2] | Philip Lovell[1] | James Turnbull[1] | Mike A. Fedak[1] | Baptiste Picard[3] | Christophe Guinet[3] | Martin Biuw[4] | Theresa R. Keates[5] | Rachel R. Holser[6] | Daniel P. Costa[2,6] | Daniel E. Crocker[7] | Patrick J. O. Miller[1]

[1]Sea Mammal Research Unit, University of St Andrews, St Andrews, UK; [2]Department of Ecology and Evolutionary Biology, University of California Santa Cruz, Santa Cruz, California, USA; [3]CNRS Centre of Biology Studies of Chizé, Villiers-en-Bois, France; [4]Institute of Marine Research, Tromsø, Norway; [5]Department of Ocean Sciences, University of California Santa Cruz, Santa Cruz, California, USA; [6]Institute of Marine Sciences, University of California Santa Cruz, Santa Cruz, California, USA and [7]Department of Biology, Sonoma State University, Rohnert Park, California, USA

Correspondence
Patrick J. O. Miller
Email: pm29@st-andrews.ac.uk

Funding information
CNES-TOSCA; DoD SERDP, Grant/Award Number: W912HQ20C0056; Institut Polaire Français Paul Emile Victor, Grant/Award Number: 109 and 1201; Office of Naval Research, Grant/Award Number: N00014-18-1-2822

Handling Editor: Sarah Marley

Abstract

1. The ability of marine mammals to accumulate sufficient lipid energy reserves is vital for mammals' survival and successful reproduction. However, long-term monitoring of at-sea changes in body condition, specifically lipid stores, has only been possible in elephant seals performing prolonged drift dives (low-density lipids alter the rates of depth change while drifting). This approach has limited applicability to other species.
2. Using hydrodynamic performance analysis during transit glides, we developed and validated a novel satellite-linked data logger that calculates real-time changes in body density (∝lipid stores). As gliding is ubiquitous amongst divers, the system can assess body condition in a broad array of diving animals. The tag processes high sampling rate depth and three-axis acceleration data to identify 5 s high pitch angle glide segments at depths >100 m. Body density is estimated for each glide using gliding speed and pitch to quantify drag versus buoyancy forces acting on the gliding animal.
3. We used tag data from 24 elephant seals (*Mirounga* spp.) to validate the onboard calculation of body density relative to drift rate. The new tags relayed body density estimates over 200 days and documented lipid store accumulation during migration with good correspondence between changes in body density and drift rate. Our study provided updated drag coefficient values for gliding ($C_{d,f}$ = 0.03) and drifting ($C_{d,s}$ = 0.12) elephant seals, both substantially lower than previous estimates. We also demonstrated post-hoc estimation of the gliding drag coefficient and body density using transmitted data, which is especially useful when drag parameters cannot be estimated with sufficient accuracy before tag deployment.

4. Our method has the potential to advance the field of marine biology by switching the research paradigm from indirectly inferring animal body condition from foraging effort to directly measuring changes in body condition relative to foraging effort, habitat, ecological factors and anthropogenic stressors in the changing oceans. Expanding the method to account for diving air volumes will expand the system's applicability to shallower-diving (<100 m) species, facilitating real-time monitoring of body condition in a broad range of breath-hold divers.

KEYWORDS
animal health, bio-logging, body density, buoyancy, marine mammal, real-time monitoring, satellite transmission

1 | INTRODUCTION

Animals have evolved to acquire resources that enable them to survive and produce viable offspring (Figure 1). Particularly for 'capital-breeding' species that fast during lactation, sufficient lipid stores are essential in determining an individual's reproductive success or failure. From this perspective, lipid store as an index of body condition is a health indicator for many animals. This view emphasizes the importance of monitoring changes in animal body condition to understand a species' life history, interactions with their environment and evolution.

Rapid data logging and telemetry developments have facilitated remote observation of animal movements and behaviour at an increasingly fine-scale (Costa et al., 2012; Hussey et al., 2015). Remote

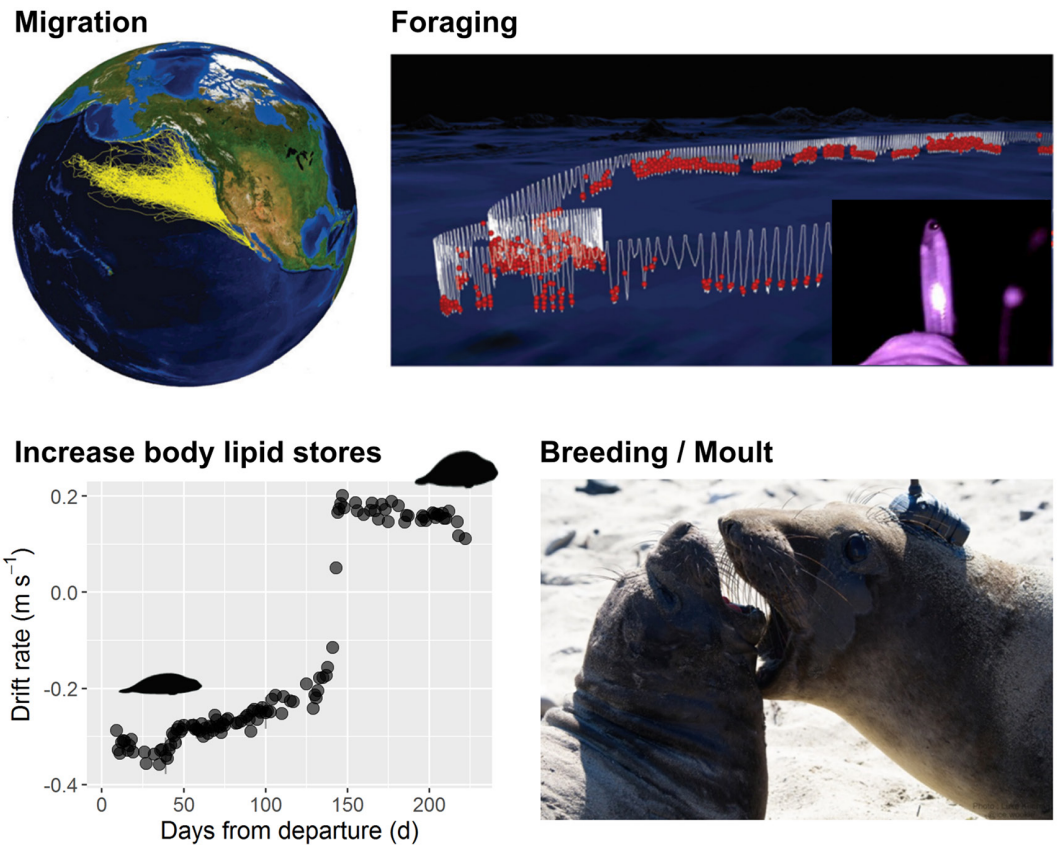

FIGURE 1 Animals collect resources to improve body condition and produce viable offspring. Northern elephant seals migrate from haul-out locations over vast areas of the North Pacific to forage upon mesopelagic fish (e.g. myctophid). As migration progresses, seals improve their body condition by increasing body lipid stores, which makes them more positively buoyant and is a vital energy store for self-survival and successful reproduction. Top figures are replicated with permission from previous studies (Adachi et al., 2021; Costa et al., 2012; Naito et al., 2013). Bottom left figure is drift rate data obtained in this study. Bottom right photo of a pup and a female northern elephant seal (with BD-SRDL on the head) was taken by Luke Keehan.

sensing techniques and in situ environmental monitoring by instruments on animals mean that their environment can also be observed at temporal and spatial resolutions appropriate to their activity. While this has enabled us to examine changes in movements and diving behaviour of diving animals in relation to various potentially important environmental characteristics, one critical underlying assumption is that specific horizontal movement characteristics (e.g. area-restricted search) and diving intensity (e.g. bottom time and dives per unit time) can be used to infer foraging. Such characteristics indicate foraging 'effort' but do not necessarily provide a reliable estimate of 'success'. More importantly, observations of at-sea foraging behaviour only are meaningful in terms of life-history success or failure if we can monitor concomitant changes in the state of the body resources that they obtain from their environment.

It is only with a clear understanding of how the nutritional state of an animal follows a trajectory required to produce offspring of sufficient quality that we can understand the fitness consequences of their behavioural and physiological responses to alterations in their environment. For example, how do we assess the implication of a shift in foraging location coincident with an anthropogenic disturbance? The consequence of the shift could range from negligible to severe, depending on how it affected a mammal's ability to successfully forage and accumulate sufficient lipid energy reserves (Keen et al., 2021; Pirotta et al., 2018). Without the ability to monitor changes in lipid-store body condition, we cannot fully judge the consequences of responses to disturbance.

In marine mammals, lipid stores are a strong predictor of survival and reproductive success of individual animals, as well as a vital property influencing thermoregulation and buoyancy control. It forms the centrepiece of the Population Consequences of Disturbance Model (National Academies of Sciences Engineering and Medicine, 2017). Although a few case studies have estimated or simulated the body condition of individual animals in response to natural and anthropogenic factors in pinnipeds and cetaceans (Costa et al., 2016; Pirotta et al., 2019; Schick et al., 2013), it remains challenging to track at-sea individual body condition in highly migratory species. There is, therefore, a critical need to develop an empirical method to monitor at-sea longitudinal changes in body condition of a range of marine mammal species. Here, in direct response to this need, we describe a novel, widely applicable tag-based system combining biologging tools with ARGOS satellite transmission to remotely monitor the lipid-store body condition of tagged animals in near real-time.

While the accumulation of lipid stores by foraging is a critical determinant of fitness in marine mammals (Arnbom et al., 1997; Fedak et al., 1996, 2009; Fleishman et al., 2016; Pomeroy et al., 1999), long-term (>months) measurements of body lipid stores of individuals have only been carried out in elephant seals (*Mirounga* spp.). Elephant seals perform 'drift dives' where they passively sink or float at depth (Crocker et al., 1997). Drift rate is the vertical rate of passive descent or ascent during the drift phase (while drifting through the water column) of 'drift dives' (Adachi et al., 2014). During the drift phase, the net buoyancy force equals the drag force at terminal speed (Aoki et al., 2011; Biuw et al., 2003) as below:

$$U_{\text{drift}} = \sqrt{\frac{\left(1 - \frac{\rho_{\text{sw}}}{\rho_{\text{seal}}}\right)mg}{0.5C_{\text{d,s}}A_{\text{s}}\rho_{\text{sw}}}}, \quad (1)$$

where U_{drift} is the drift rate (m s^{-1}) either descending with negative buoyancy or ascending when the seal has net positive buoyancy, ρ_{sw} is the surrounding seawater density (kg m^{-3}), ρ_{seal} is the body density of the seal (kg m^{-3}), m is the mass of the seal (kg), g is the gravity (m s^{-2}), $C_{\text{d,s}}$ is the drifting drag coefficient based on the total surface area of the seal (dimensionless) and A_{s} is the total surface area of the seal (m^2) calculated from the girth and length measurements in assuming that the seal is a prolate spheroid (as per Biuw et al., 2003). Drift rate has therefore been used as an effective parameter reflecting elephant seals' body density (Aoki et al., 2011; Biuw et al., 2003). This method only requires low sampling rates of depth to quantify drift rate, which changes with body lipid stores (Figure 1) (Adachi et al., 2014, 2021; Beltran et al., 2021; Biuw et al., 2003, 2007; Richard et al., 2014; Robinson et al., 2010, 2012). However, most marine mammals do not regularly exhibit similar drift dives. Thus, this method does not apply to species other than elephant seals. A few other pinnipeds, such as Baikal seals (*Pusa sibirica*; Watanabe et al., 2015), hooded seals (*Cystophora cristata*; Andersen et al., 2014) and New Zealand fur seals (*Arctocephalus forsteri*; Page et al., 2005) conduct drift dives, but the drift dives are less frequent in such species, limiting our ability to extend the drift dive method beyond elephant seals.

In response to the limitations in the applicability of the drift dive method, an alternative tag-based approach was developed that uses 'gliding' behaviour during descent and ascent transit phases of dives, ubiquitous in diving animals (Williams et al., 2000), to estimate lipid stores (Aoki et al., 2011; Miller et al., 2004, 2016). Here, we only use the term 'glide' to refer to times when animals cease stroking, and glide along their swimming path, so acceleration (a) is determined solely by external drag and buoyancy forces. It is expressed as:

$$a = -\frac{C_{\text{d,f}}A_{\text{f}}}{m}0.5\rho_{\text{sw}}U^2 + \left(\frac{\rho_{\text{sw}}}{\rho_{\text{seal}}} - 1\right)g\sin\theta, \quad (2)$$

where a is the change in speed during the glide (i.e. acceleration; m s^{-2}), $C_{\text{d,f}}$ is the gliding drag coefficient based on the frontal area of the seal (dimensionless), A_{f} is the frontal area of the seal (m^2) calculated from the girth measurement in assuming that the seal is circular in cross-section as per Aoki et al. (2011), m is the mass of the seal (kg), ρ_{sw} is the surrounding seawater density (kg m^{-3}), U is the swim speed during the glide, ρ_{seal} is the body density of the seal (kg m^{-3}), g is the gravitational constant ($9.8\,\text{m s}^{-2}$) and θ is the body pitch angle of the seal during the glide. Note that m, ρ_{sw}, ρ_{seal} and g are shared with Equation (1).

The glide-based method is potentially applicable to most marine mammals. Still, it requires a high sampling rate of depth and three-axis acceleration data to separate gliding from stroking behaviour, and to estimate the parameters in Equation (2) to describe speed performance (a, U) and pitch angle (θ) during glides. The glide-based approach has only been implemented using short-duration archival data to obtain cross-sectional 'snapshots' of body density

(e.g. Aoki et al., 2021), and has not been used to track longer-term longitudinal changes in lipid-store body condition.

This study aimed to develop and demonstrate a novel onboard algorithm on a new type of satellite-linked data logger; the 'Body Density Satellite Relay Data Logger' (hereafter, abbreviated BD-SRDL). These data loggers are produced by the Sea Mammal Research Unit Instrumentation Group (SMRU-IG), St Andrews, Scotland, and were based on the general design principles of standard SMRU-IG SRDLs (Fedak, 2013; Fedak et al., 2001) but with additional hardware memory and entirely new onboard data sampling and processing systems to sample both depth and three-axis acceleration. In addition to the parameters available on the standard SMRU-IG SRDLs, these data loggers were designed to calculate and telemeter body density (as an index of lipid-store body condition) via the ARGOS satellite system in near real time, as well as to archive raw data to be recovered when the seals returned to shore. First, an onboard algorithm was implemented to calculate the body density of elephant seals following Equation (2), using analysis of glides during the descent and ascent phases. Because the tag had to be placed on the head of seals to enable satellite telemetry, it was necessary to calculate a correction factor for animal pitch as measured on the head versus back of elephant seals. In addition, surrounding seawater density was estimated based on each glide's depth, using upon analysis of CTD (conductivity, temperature and depth) casts previously made in the geographical area where the seals foraged.

In total, 24 elephant seals (with over 1200 data days) were used to develop, test and validate the body density algorithm. Seven free-ranging northern elephant seals were tagged with prototype versions of the BD-SRDL running the algorithm onboard for real-time monitoring of the body density changes. Nine free-ranging southern elephant seals were tagged with high-rate archival DTAGs (Johnson & Tyack, 2003), obtaining the entire high sampling rate data records with which both drift rates and body density could be calculated. Three translocated northern elephant seals were tagged with high-rate archival accelerometers, conducting experimental body density manipulation. Five free-ranging southern elephant seals were tagged with head- and back-attached archival accelerometers for head-to-back pitch angle correction. We assumed that the pitch angle correction parameters obtained from southern elephant seals apply to northern elephant seals, as they are two closely related species with similar morphology and diving behaviour. A simulated version of the onboard algorithm was used to analyse all archival datasets, enabling body density estimates to be validated against drift rates. As they are important parameters to calculate body density (Equations 1 and 2), updated drag coefficients for gliding ($C_{d,f}$ in Equation 2) and drifting ($C_{d,s}$ in Equation 1) were estimated by determining which values provided a best fit to the body density and drift rate datasets, and further validated by a separate analysis of terminal gliding speeds (Watanabe et al., 2006).

Our novel onboard body density tracking and telemetry approach worked effectively to track body density changes of elephant seals for over 200 days, using the BD-SRDL. As this system is designed to also be applicable to other deep-diving marine mammals, our study represents a breakthrough to enable at-sea body condition monitoring in many marine mammals.

2 | MATERIALS AND METHODS

2.1 | Body density satellite relay data logger

The novel BD-SRDL was based on the standard SRDL developed and manufactured by the SMRU-IG, which is described in detail in Fedak (2013) and Fedak et al. (2001). Signal processing and conditioning was implemented on a microcontroller with 32 kByte RAM and an ARM Cortex-M4 CPU. The CPU has a floating-point hardware accelerator that enables high-efficiency, low-power, single-precision signal processing (see Supporting Information for the full technical description of BD-SRDL).

2.2 | Onboard body density algorithm

To estimate body density in real time, an onboard algorithm to solve Equation (2) for ρ_{seal} was implemented on the BD-SRDL described above. The body density algorithm is implemented on the onboard microcontroller to derive a ρ_{seal} value for each glide based on tag measurements using high sampling rate depth and three-axis acceleration data (Figure 2). The same procedure was used for the simulation experiment emulating the onboard algorithm on archived data. 40 Hz depth and 128 Hz 3-axis acceleration data were processed onboard to derive 5 Hz depth, swimming effort and pitch estimates and hence to identify short passive glide segments (i.e. 5-second sub glide; hereafter, referred to as '5-s-glide'). The choice of a duration of 5 s was based on its effectiveness in previous studies (Aoki et al., 2011; Miller et al., 2016). 5 Hz depth and pitch estimates were used to quantify in situ gliding acceleration (a), swim speed (U) and average pitch angle (θ) per 5-s-glide. Adding a value for seawater density (ρ_{sw}) enabled solving Equation (2) to obtain a body density estimation (ρ_{seal}) for each 5-s-glide. The gliding drag coefficient ($C_{d,f}$) was initially set to 0.19 based on Aoki et al. (2011), but later updated to 0.03 for all seals based on empirical findings in this study as detailed in the later section. Individual specific values of frontal surface area (A_f) and mass (m) were set per each seal based on direct field measurements of weight and circumference (Table 1). The last remaining gravity parameter (g) was constant at 9.8 m s^{-2}.

2.3 | Data processing steps of the onboard algorithm

Depth and three-axis acceleration were measured with tags attached on the head of seals (Figure S1). Data were processed onboard (Figure 2b; also see Supporting Information for details of

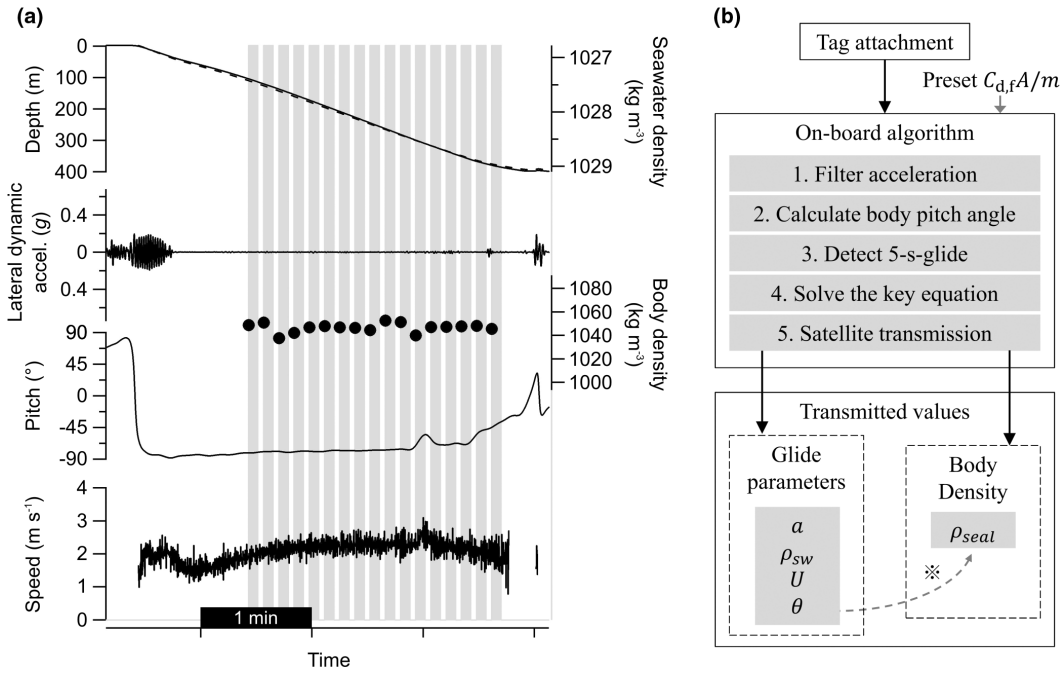

FIGURE 2 Schematic of the onboard algorithm on Body Density Satellite Relay Data Logger (BD-SRDL). (a) Time-series example of glide parameters used to calculate a body density (ρ_{seal}) value for each 5-s-glide. Depth, lateral dynamic acceleration, pitch (θ) and swim speed (U; calculated only with pitch >|30°|) are shown as solid black lines. Seawater density (ρ_{sw}) is shown as a dotted black line. Calculated body density values are shown as filled black circles. Each 5-s-glide is shown as grey shade, where depth is >100 m, no stroke was detected and pitch was over |30°| (later updated to |50°|). (b) Conceptual flowchart of the method (see Supporting Information for a technical description of implementation). ※The grey dotted line at bottom represents post-hoc calculation of body density with transmitted glide parameters enabling an updated value of drag coefficient term $C_{d,f}A_f/m$.

onboard processing procedures) and analysed using a simulator for archived datasets as follows:

1. **Acceleration filtering**

   Three-axis accelerations (longitudinal surge, lateral sway and dorsoventral heave acceleration) were filtered to separate accelerations into two components: static (lower frequency) acceleration related to the posture of the seal relative to gravity (e.g. pitch angle) and dynamic (higher frequency) acceleration, primarily created by flipper strokes to generate thrust. Here, static accelerations were obtained using a low-pass filter of 0.2 Hz. Dynamic accelerations were obtained using a bandpass filter of 0.43–1 Hz. The filtering processes were conducted independently on each axis of three-axis acceleration.
2. **Calculation of body pitch angle from head measurements**

   Diving seals tend to adopt a consistent posture while swimming to maintain a body shape that minimizes drag. Because the BD-SRDLs need to be mounted on the heads of animals to maximize the number of successful transmissions, we established the relationship of the pitch measured on the head-mounted device to the pitch of the long axis of the animals' body, using identical loggers mounted on the head and body of female southern elephant seals. Archival acceleration data were obtained from free-ranging adult female southern elephant seals (dataset 1; $n=5$) and were used for head-to-back pitch angle correction (Table 1). This fieldwork was conducted at Kerguelen Islands (49°20′S, 70°20′E) during the breeding season. It covered the 2-month post-breeding foraging migration (October–January) from 2010 to 2013. Each seal was chemically immobilized using a standard protocol (Mcmahon et al., 2000). Tags were attached, and body mass and morphometric measurements were collected just before seals departing to sea at the end of the breeding season. Upon return for the annual moult after their post-breeding foraging migrations, seals were again chemically immobilized to recover the data loggers. The five seals were each equipped with two archival tags, one on the head (MK10-X; Wildlife Computers) and another on the back (TDR10-Daily Diary tag; Wildlife Computers) placed in a consistent position on the animal using a quick-setting epoxy glue (Araldite AW 2101). The tags had a depth (pressure) sensor (sampled at 1 Hz) and a three-axis accelerometer (sampled at 16 Hz).

   The head-back pitch correction factor used three-axis acceleration data from head-attached and back-attached tags on the same individuals as detailed above. The key correction factor is the inclination angles of head-attached tags relative to back-attached tags. If the head-attached tag was perfectly aligned with the back-attached tag, the inclination angles should be 0 in all three axes. Here, we validated that the head-attached tags were inclined +24° the longitudinal (surge) axis relative to the back-attached tags (Figure S2A) by the following steps: (i) three-axis head accelerations were filtered to obtain static accelerations using the

TABLE 1 Dataset summary of 24 female elephant seals (*Mirounga* spp.), listed in chronological order of years tagged.

				Tagging information					
								Sampling rate (Hz)	
Dataset ID	Tagged year	Species (−elephant seal)	Seal ID	Setting	Data type	Tagging position	Data usage	Depth	Accel.
1	2010	Southern	2010-21	Free-ranging	Archival	Back & Head	Pitch correction	1	16
	2012		2012-9						
	2013		2013-11						
	2013		2013-12						
	2013		2013-16						
2	2017	Southern	ml17_280a	Free-ranging	Archival	Head	Algorithm validation & $C_{d,f}$, $C_{d,s}$ estimation	5	25
	2017		ml17_281a						
	2017		ml17_301a						
	2018		ml18_292a						
	2018		ml18_294a						
	2018		ml18_294b						
	2019		ml19_292a						
	2019		ml19_293a						
	2019		ml19_295a						
3	2019	Northern	H002-12776	Trans-location	Archival	Head	Algorithm validation	5	25
	2019		H005-12779						
	2019		H006-15055						
4	2020	Northern	Prototype-1_20006						
	2020		Prototype-1_20007						
5	2021	Northern	Prototype-1_20002	Free-ranging	Archival & Satellite	Head	On-board body density calculation, satellite transmission, & $C_{d,s}$ estimation	40	128[b]
	2021		Prototype-2_20003						
	2021		Prototype-2_20008						
	2021		Prototype-2_20010						
	2021		Prototype-2_20011						

[a]Prolonged glide was not quantified due to translocating experiment (dataset 3) or paucity of archival acceleration data (datasets 4 and 5).
[b]Archival data are not available.
[c]Shallower pitch threshold was applied for dataset 4.
[d]Pitch threshold, glide statistics, drift dive statistics and field measurements were irrelevant and not applied for the usage of the dataset 1.

same method as in Step 1 of the onboard algorithm, (ii) the static accelerations were processed using a right-handed rotation matrix based on Johnson and Tyack (2003) with inclination angles of pitch, roll and heading (i.e. +24, 0, 0, respectively) to obtain head-corrected static accelerations and (iii) head-corrected static accelerations were used to calculate corrected head pitch angle by

$$\theta = \operatorname{atan}\left(\frac{\mathrm{Surge}_{\mathrm{static}}}{\sqrt{\left(\mathrm{Sway}^2_{\mathrm{static}} + \mathrm{Heave}^2_{\mathrm{static}}\right)}}\right), \quad (3)$$

where $\mathrm{Surge}_{\mathrm{static}}$, $\mathrm{Sway}_{\mathrm{static}}$ and $\mathrm{Heave}_{\mathrm{static}}$ are static accelerations in three axes.

To investigate the one-to-one relationship between body pitch angle (calculated with back-attached tags by Equation 3) and head-corrected pitch angle, we only used data during transit phase (i.e. descent and ascent phase, defined as per Miller et al. (2004) where dive was defined as deeper than 10 m depth as per Adachi et al. (2021)). We extracted 70 million synchronized data points from four seals. These data were randomly subsampled to 10% of their original to conduct a simple linear regression of body-mounted pitch angle against head-mounted pitch angle using the *biglm* function in the BIGLM package distributed via R (Lumley, 2013), confirming that the inclination of +24° gives us a good estimates of animal body pitch angle from head-attached tags (r^2=0.97; Figure S2B).

3. Detecting 5-s-glides

Each 5-s-glide segment was detected in real time using the following steps. First, any 2-s time window meeting the following two criteria were detected: (i) depth >100 m to minimize the

						Field measurements					
						Deployment			Recovery		
Data duration (d)	Pitch threshold (degree)	ρ_{sw} during 5-s-glides (kg m^{-3})	Total no. of 5-s-glides (*n*)	Total no. of drift dive (*n*)	Total no. of prolonged glide (*n*)	Mass (kg)	Girth (m)	Length (m)	Mass (kg)	Girth (m)	Length (m)
69	n/a[d]										
19											
25											
21											
16											
30	50	1028.7 ± 0.9	35,636	98	322	395	1.84	2.35	n.d.		
37		1029.4 ± 1.3	52,336	65	240	547	2.05	2.52			
37		1028.2 ± 0.5	26,029	108	156	417	1.85	2.50			
31		1028.4 ± 0.9	18,162	123	190	238	1.58	2.26			
31		1028.3 ± 0.7	26,112	78	90	238	1.58	2.26			
28		1028.3 ± 0.9	16,057	129	118	303	1.67	2.30			
29		1028.5 ± 0.9	26,729	118	124	235	1.63	2.35			
31		1028.4 ± 0.8	24,337	112	208	307	1.72	2.47			
22		1028.4 ± 1.0	13,658	83	124	288	1.62	2.39			
0.8	50	1026.6 ± 0.2	36	0	n/a[a]	109	1.22	1.66	n.d.		
1.9		1026.7 ± 0.4	59	1		118	1.23	1.61			
4.9		1027.1 ± 0.6	3230	24		162	1.07	1.91			
223	30[c]	1027.8 ± 0.9	77,532	123	n/a[a]	319	1.64	2.66	468	1.98	2.76
227		1027.8 ± 1.0	79,484	158		280	1.57	2.66	468	2.07	2.73
82	50	1027.8 ± 1.0	67,712	23		372	1.80	2.79	459	2.09	2.82
80		1027.8 ± 1.0	45,040	42		316	1.67	2.66	377	1.97	2.66
71		1027.9 ± 1.1	83,576	39		326	1.80	2.47	313	1.71	2.45
74		1027.8 ± 1.0	70,740	20		328	1.90	2.60	391	2.05	2.62
76		1027.4 ± 0.9	36,630	21		325	1.79	2.63	399	2.01	2.62

effect of lung gas volume on total animal buoyancy and (ii) root mean square of sway dynamic acceleration <0.05G to remove any stroking phase. When (i, ii) are met, a consecutive 5-s window meeting the following three criteria were detected: (iii) depth >100 m (same as criterion i), (iv) root mean square of sway dynamic acceleration <0.05G (same as criterion ii) and (v) absolute pitch angle $|\theta| > 50$ (or 30) degrees for calculating speed ($U = \triangle\text{Depth}/\sin\theta$). The remaining glide parameters in Equation (2) were quantified as follows: a during 5-s-glides was calculated as the slope of a linear regression of swim speeds against time within the 5-s window; U and θ are the averaged values of swim speed and body pitch angle, respectively, during the 5-s-glides.

A value for seawater density ρ_{sw} for each glide was specified based on typical seawater density at each glide depth. We obtained seawater temperature and salinity data along depth through the World Ocean Database (https://www.nodc.noaa.gov/OC5/SELECT/dbsearch/dbsearch.html) (Boyer et al., 2018). From the database, we obtained all available profiling float data during 2015–2020 in the northeast Pacific Ocean for northern elephant seals (longitudes of −180° to −120° and latitudes of 30°–60° without the region of Bering Sea; 657 casts in total) and in the Southern Ocean for southern elephant seals (longitudes of 20°–140° and latitudes of −70° to −40°; 1341 casts in total), which corresponds to where our study species potentially migrated and dived as per previous studies that conduct animal tracking (Bailleul et al., 2007; Guinet et al., 2014; Robinson et al., 2012). Then, we calculated seawater density ρ_{sw} versus depth (as in Aoki et al., 2011) and fitted a power curve of density against depth for all data points from the northeast Pacific Ocean and

the Southern Ocean, respectively (Figure S3). Average depth during each 5-s-glide was used to estimate ρ_{sw}.

4. **Solving the key equation**

   Using glide parameters, ρ_{seal} for each 5-s-glide was calculated by solving Equation (2). Glide parameters (a, ρ_{sw}, U, and θ) and ρ_{seal} were stored in the BD-SRDLs onboard memory.
5. **Satellite transmission**

   Glide parameters (a, ρ_{sw}, U and θ) and ρ_{seal} were transmitted as frequently as allowed by the ARGOS system when seals were at the surface. See Supporting Information and Fedak et al. (2001) for the technical description of transmission scheduling.

2.4 | Datasets used for developing and validating the algorithm

Table 1 describes all datasets used in this study. Dataset 2 through 5 ($n=19$ tag records) were used to develop and validate the onboard algorithm. Datasets 2 and 3 were obtained from archival accelerometers to simulate the onboard algorithm in desktop PC simulations of the onboard algorithm and traditional analysis methods (Aoki et al., 2011). Datasets 4 and 5 were obtained from field deployments of the newly developed BD-SRDL running the onboard algorithm on northern elephant seals, allowing us to evaluate onboard glide selection and body density estimation using archived and satellite-transmitted data.

Fieldwork on northern elephant seals was conducted at the University of California Natural Reserve System's Año Nuevo Reserve under NMFS (National Marine Fisheries Service) permit No. 14636 and 19,108 issued to D. P. Costa and was approved by the Institutional Animal Care and Use Committee (IACUC) at UCSC. Fieldwork on southern elephant seals was conducted at Kerguelen Island, financially and logistically supported by the IPEV (Institut Paul Emile Victor) under the Antarctic research program 109 (C. Barbraud) and 1201 (C. Gilbert & C. Guinet) and CNES-TOSCA as part of the SNO-MEMO.

2.4.1 | Field deployments of BD-SRDL

For the final evaluation of the onboard algorithm, archived and satellite-transmitted data (datasets 4 and 5; $n=7$) were obtained from the BD-SRDLs attached to free-ranging adult female northern elephant seals (Table 1). Fieldwork was conducted at Año Nuevo State Park, CA, USA (37°50′N, 122°16′W) during the seals' breeding and moulting season. The 7-month post-moulting foraging migrations occurred from June to January in 2020–2021 ($n=2$), and the 2-month post-breeding migrations occurred from February to May in 2021 ($n=5$). Each seal was chemically immobilized using a standard protocol (Robinson et al., 2012) to attach the data loggers and to collect body mass and morphometric measurements at deployment. Seals were chemically immobilized after their foraging migrations to recover the data loggers. The seven seals were equipped with the BD-SRDLs, attached to the fur on the head using 5-min epoxy with high-tension mesh netting and cable ties (Figure 1; Figure S1). The tags had depth (pressure) sensors (sampled at 40 Hz) and a three-axis accelerometer (sampled at 128 Hz). The tags run the onboard algorithm, enabling onboard calculation and satellite transmission of body density estimates with glide parameters based on steps 1–4 of the onboard algorithm. Also, the tags stored the gliding parameters of all detected 5-s-glides and a complete time series of raw depth data (stored at 1 and 5 Hz in 2020 and 2021 deployments, respectively), to be used for validation analyses and more frequent estimates of body density.

We conducted field tests of the BD-SRDL twice to enable improvements between the two prototypes. The onboard algorithm running on Prototype-1 (2020) and Prototype-2 (2021) were only different in terms of pitch thresholds; 30 and 50 degrees for Prototype-1 and Prototype-2, respectively (see Step 3 of the onboard algorithm). This change in pitch threshold setting was done after detailed effects of the pitch angle were investigated using dataset 2, which included high-sampling raw depth and three-axis acceleration archival data from free-ranging seals (Table 1).

2.4.2 | High-sampling archival data using DTAGs

Archival data obtained from free-ranging adult female southern elephant seals (dataset 2; $n=9$) were used for validation of the onboard algorithm and estimation of drag coefficients ($C_{d,f}$ in Equation 2 and $C_{d,s}$ in Equation 1) (Table 1). Fieldwork was conducted at Kerguelen Islands during the elephant seal breeding seasons from 2017 to 2019, to examine the 2-month post-breeding foraging migrations (Goulet et al., 2019, 2020), with the same standard protocol as dataset 1. The nine seals were equipped with high-sampling archival accelerometers (DTAG, SMRU-IG) on the head. Similar to the BD-SRDLs, these DTAGs have a depth (pressure) sensor (downsampled from 25 Hz to 5 Hz) and a tri-axis accelerometer (downsampled from 200 Hz to 25 Hz).

2.4.3 | Archival accelerometers used with body density manipulation during translocations

Archival data obtained from translocating juvenile northern elephant seals (dataset 3; $n=3$) were used to validate the onboard algorithm (Table 1). Fieldwork was conducted at Año Nuevo State Park, CA, USA, in October 2019 to conduct translocation experiments with body density manipulation. Each seal was chemically immobilized using a standard protocol (Robinson et al., 2012) and transported to Long Marine Laboratory (Santa Cruz, CA, USA), where they were kept overnight for (i) collection of body mass and morphometric measurements, (ii) instrument attachment and (iii) weight attachment to manipulate body density of the animals. The three seals were equipped with high sampling rate archival SMRU tags (SMRU-IG) on the head using 5-min epoxy with high-tension mesh netting and cable ties. The tags sampled depth at 5 Hz and three-axis acceleration at 25 Hz. A cuboid weight (3.63 kg

in air) was also attached on the back of each seal to experimentally manipulate its body density. The weight was tied with a time-scheduled release mechanism (Little Leonardo Co.) to automatically release the weight at sea, making seals experience two body density conditions: weighted and unweighted conditions for higher and lower body density. The release time was set as 12 h (for Seal ID: H002-12776 and H005-12779) and 18 h (for Seal ID: H006-15055) after deployment. The seals were transported by boat to a release site above the Monterey submarine canyon, as in Aoki et al. (2011). Seals were chemically immobilized upon return from the sea to recover the data loggers.

2.5 | Validations of onboard body density estimates

The onboard body density estimates were validated using three methods; (1) desktop version of algorithm for body density estimation, (2) drift rate and (3) terminal speed at descent of prolonged glides. Details of each validation method are described in the following sections.

2.5.1 | Desktop version of the algorithm for body density estimation

To validate the performance of the onboard algorithm, we built a desktop version of the body density algorithm. This version utilized the most detailed and accurate method of detecting glides based on Aoki et al. (2011). This validation was conducted using the DTAG dataset from southern elephant seals (dataset 2; Table 1). We analysed time-series data per day per individual a step-wise process described below. Except for Step 1, each step is comparable to our onboard algorithm described above. The desktop analyses are more fine scale because they determine daily- and individual-specific configurations for the filtering acceleration, rather than using the fixed values across days and individuals (see Step 1 of the onboard algorithm). Below is the outline of the desktop version of the algorithm.

1. **Acceleration filtering**

   Power spectral density (PSD) was calculated from raw lateral acceleration data during dives >10 m depth (Adachi et al., 2021), using the built-in function *PowerSpectralDensity* in IGOR Pro v. 6.04 (WaveMetrics Inc.) based on our previous studies (Adachi et al., 2017; Aoki et al., 2011). The PSD showed a dominant stroke frequency together with a clear trough (e.g. see figure 1c of Sato et al., 2007), which is considered to represent the boundary between slower static and faster dynamic components of acceleration. Using the trough value from the PSD from each day, a low-pass filter was applied to all three axes to obtain static accelerations, using the built-in *FilterFIR* in IGOR Pro. The static accelerations were subtracted from the raw accelerations to obtain dynamic accelerations.
2. **Calculation of body pitch angle from head measurements (same as Step 2 of the onboard algorithm)**
3. **Detecting 5-s-glides (same as Step 3 of the onboard algorithm)**
4. **Solving the key equation (same as Step 4 of the onboard algorithm)**

   Note that $C_{d,f}$ was set as 0.03 (same as the onboard algorithm) based on simulations using empirical data, as detailed in the later sections.

2.5.2 | Quantification of drift rate to validate body density in elephant seals

To evaluate the empirical correlations between drift rate and body density, we calculated drift rate for datasets 2 through 5 (Table 1). First, we visually inspected time-series data of depth and accelerations during drift dives in translocated seals (dataset 3). We wrote custom-written codes for the automated calculation of drift rates based on the visual inspection and previous studies, as detailed below.

1. **Drift rates from translocation seals with body density manipulation**

   Since the number of drift dives is limited in dataset 3 due to the short duration of the trials (Table 1), we manually detected drift dives and calculated drift rates using four criteria based on previous studies: (i) a drift dive has the distinctive 'drift dive' profile (Crocker et al., 1997), in which the shallowest depth of a drifting phase is (ii) deeper than 100 m, to minimize the effect of lung gas volume on buoyancy (Adachi et al., 2021), (iii) without any strokes (Adachi et al., 2014), and (iv) where seals are in a belly-up orientation (i.e. heave static acceleration is nearly −1G) (Mitani et al., 2010). In total, 25 drift dives were obtained from the three seals (Table 1). As detailed below, the visually confirmed criteria were implemented into the custom-written codes for the automated calculation of drift rates in other datasets.
2. **Drift rate determined from free-ranging seals with DTAGs**

   Based on the visual inspection of translocation seals above, we developed custom-written code, updating the method by Adachi et al. (2021) as follows: A drift phase must (i) have depths >100 m, (ii) be longer than 20% of the total duration of the drift dive, (iii) have little variance in depth change rate during the entire drift phase (i.e. mean squared residual should be less than 3 m^2), (iv) include no strokes, and (v) have heave static acceleration <0 (to choose sideways to belly-up body orientations observed during drifting). We applied this method to dataset 2, in which archival three-axis acceleration data were available to apply the above criteria (iv) and (v). In total, 914 drift dives were obtained from the nine seals in dataset 2 (Table 1).

3. **Drift rate determined from free-ranging seals with the BD-SRDL** BD-SRDL only stored depth data as archival time series (Table 1), so any criteria related to acceleration signals could not be applied in archival analyses. Here, based on the empirical observation on the dive profiles and those of previous studies (Beltran et al., 2021; Crocker et al., 1997; Naito et al., 2013), the acceleration criteria (iv and v) in the last section were replaced by adding one other criterion and two additional filtering steps in the custom-written code; (i–iii) the same criteria as in the last section were applied, and (iv) a drift phase has no wiggles (i.e. depth change is always negative/positive during a drift phase). Two additional filtering steps were applied by (v) obtaining a median value of drift rates in consecutive drift dives that occurred at least three times in a row, and (vi) auto-calculated drift rates (calculated using criteria i–v) were post-processed by a Kalman filter proposed by Arce et al. (2019) to remove outliers. In total, 426 drift dives were obtained from the seven seals (Table 1).

2.5.3 | Using terminal glide speed to validate estimates of gliding drag coefficient $C_{d,f}$

When negatively buoyant, seals perform prolonged glides during the descent phase, where the drag force equals the magnitude of buoyancy along the swimming path as below (Aoki et al., 2011);

$$U_{ter} = \sqrt{\frac{\left(\frac{\rho_{sw}}{\rho_{seal}} - 1\right) mg\sin\theta}{0.5 C_{d,f} A_f \rho_{sw}}}, \quad (4)$$

where U_{ter} is the terminal speed ($m\,s^{-1}$) in the descent phase. Note that other parameters are shared with Equation (2). Terminal speed is an effective parameter for estimating the body density of elephant seals (Aoki et al., 2011) and other seals (e.g. Baikal seals; Watanabe et al., 2006). Here, we identified prolonged descent glides and calculated terminal speed using three criteria based on Aoki et al. (2011): a prolonged descent glide (i) has no depths less than 100 m (to minimize the effect of gases in the lungs on buoyancy), (ii) is longer than 40 s, (iii) has maximum swim speed (i.e. terminal speed) and maximum absolute pitch angle within 20 s prior to the end of the prolonged glide (i.e. reached a terminal speed around the end of the prolonged glide). The calculation of terminal speed was conducted on dataset 2, including 1572 prolonged glides in total from the nine seals (Table 1). The terminal speed was used to evaluate the empirical correlation with body density and estimate unknown drag coefficients as detailed in the following paragraphs.

We used terminal speed to estimate $C_{d,f}$ (gliding drag coefficient based on the frontal area of the seal), which is a key unknown parameter in Equation (2) to estimate body density. Specifically, the same drag coefficient ($C_{d,f}$) is shared in Equations (2) and (4), enabling us to estimate $C_{d,f}$ based on the correlation between empirical terminal speed and theoretical terminal speed. Here, $C_{d,f}$ was simulated with the range of 0.01–1 to cover the reported values (0.17–0.26) estimated in the previous study (Aoki et al., 2011). The best-fit $C_{d,f}$ was determined per individual of the dataset 2 (Figure 3a) by the following six steps:

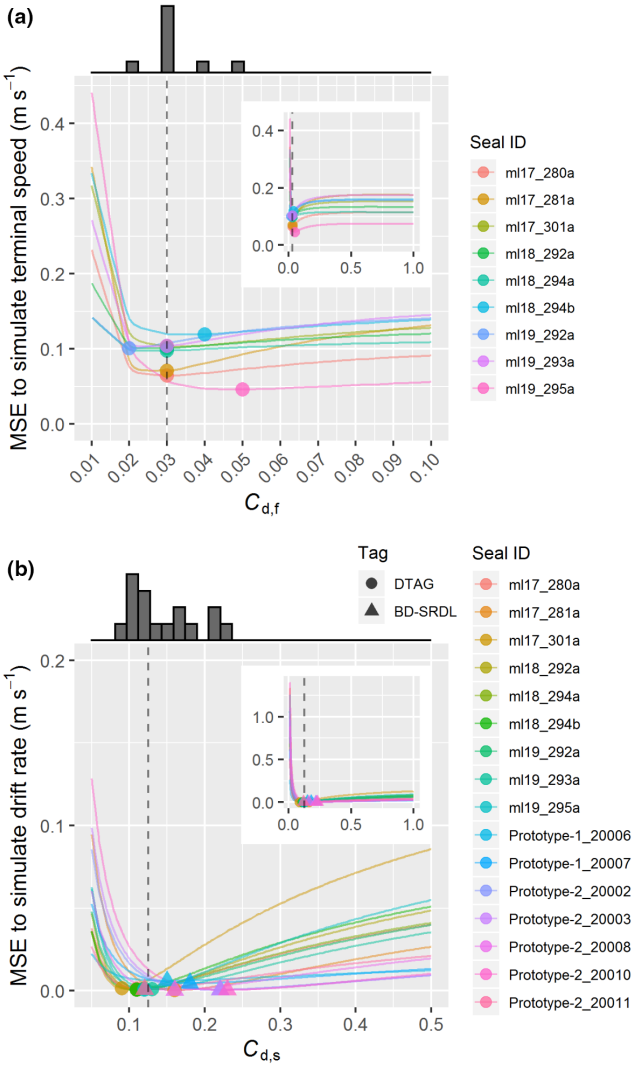

FIGURE 3 Drag coefficients estimation. (a) A gliding drag coefficient $C_{d,f}$ and (b) a drifting drag coefficient $C_{d,s}$ were estimated using empirical terminal speed U_{ter} and drift rate U_{drift}, respectively. Vertical dashed lines show the selected value (i.e. median).

1. **Compile a list of all prolonged glides:** list all detected prolonged glides and empirical terminal speed based on the method in the last section,
2. **Select a value of $C_{d,f}$** : select and fix a value of $C_{d,f}$ (ranging from 0.01 to 0.1, by 0.01 increments) for the next steps 3 and 4,
3. **Simulate ρ_{seal} using Equation (2) with a focal $C_{d,f}$**: at a prolonged glide, identify all 5-s-glides within 4-h windows centred on a start time of the prolonged glide, and calculate averaged ρ_{seal} from the 5-s-glides using the key Equation (2),
4. **Simulate U_{ter} using Equation (4) with the ρ_{seal} value and a focal $C_{d,f}$**: calculate theoretical terminal speed per prolonged glide using Equation (4) with the averaged ρ_{seal} obtained in the last step 3,

5. **Repeat steps 2–4**: simulate ρ_{seal} and U_{ter} for all detected prolonged glides (listed in step 1) with all combinations of $C_{d,f}$,
6. **Determine the best-fit $C_{d,f}$**: calculate mean squared errors (MSEs) between empirical terminal speed and simulated terminal speed per $C_{d,f}$, and finally determine the $C_{d,f}$ value that has the lowest MESs, defined as the best-fit $C_{d,f}$ per individual.

The median of best-fit gliding drag coefficient $C_{d,f}$ was 0.03 (with the individual variation of 0.02–0.05) (Figure 3a), which is one order of magnitude lower than the previously reported values (0.17–0.26) in juveniles with a mean body mass of 172 kg (Aoki et al., 2011). Hereafter, for further results, the median value of 0.03 was used to estimate body density to solve Equation (2) (as noted in the above sections *2.2 Onboard body density algorithm* and *2.5.1 Desktop version of the algorithm for body density estimation*).

2.6 | Determine the drifting drag coefficient $C_{d,s}$

$C_{d,s}$ (a drifting drag coefficient based on the total surface area of the seal) in Equation (1) was also unknown. Still, combining Equations (1) and (2) with $C_{d,f}=0.03$ (as determined above) enabled us to estimate the $C_{d,s}$ for each individual. Here, $C_{d,s}$ was simulated across the range of 0.01–1 to cover the value (0.69) estimated in the previous study (Biuw et al., 2003). Note that $C_{d,s}$ was simulated daily because a daily scale is an appropriate time scale in terms of rates of change to analyse drift dives in free-ranging seals based on previous studies (Adachi et al., 2014, 2021; Beltran et al., 2021; Biuw et al., 2003, 2007; Richard et al., 2014; Robinson et al., 2010, 2012). Then, the best-fit $C_{d,s}$ was determined per individual of the datasets 2, 4 and 5 (Figure 3b) by the following four steps:

1. **Compile a list of all days that include drift dives:** list all days including at least one drift dive and calculate empirical daily averaged drift rates,
2. **Select a value of $C_{d,s}$**: select and fix a value of $C_{d,s}$ (ranging from 0.01 to 0.1, by 0.01 increments) for the next step 3,
3. **Simulate U_{drift} using Equations (1) and (2) with the ρ_{seal} value and a focal $C_{d,s}$**: for each day, identify all 5-s-glides and use them to calculate a daily averaged value of ρ_{seal} using Equation (2) (with $C_{d,f}=0.03$). Then, calculate the theoretical drift rate per day using Equation (1) with the daily averaged ρ_{seal},
4. **Repeat Steps 2 and 3**: simulate U_{drift} for all days (listed in step 1) with all combinations of $C_{d,s}$,
5. **Determine best-fit $C_{d,s}$**: calculate MSEs between empirical drift rate and simulated drift rate per $C_{d,s}$, and finally determine the $C_{d,s}$ value with the lowest MSEs, defined as the best-fit $C_{d,s}$ per individual.

The median of best-fit drifting drag coefficient $C_{d,s}$ was 0.12 (with an individual variation of 0.09–0.23) (Figure 3b), which is substantially lower than the previously reported value (0.69) in newly weaned pups with a mean body mass of 92.5 kg (Biuw et al., 2003). The 0.12 value was then used to relate drift rates to body density.

3 | RESULTS

3.1 | Validation of body density algorithm versus drift rates in free-ranging seals

Field tests of two prototypes of BD-SRDLs were conducted in 2020 ($n=2$; dataset 4) and 2021 ($n=5$; dataset 5) in free-ranging northern elephant seals using the onboard algorithm in the tags to calculate body density values and transmit them via satellite, while concurrently having the tags store raw data for subsequent post-processing. The tags were recovered when the animals returned to shore. The stored data were post-processed to calculate body density and drift rate. A simulated version of the onboard algorithms was also applied to data obtained from recorders on southern elephant seals (dataset 2). The hardware of the two prototypes was identical. Still, the onboard algorithm was modified to increase the pitch threshold from 30° to 50° in Prototype-2 (2021; see Table 1) to reduce variability in body density estimates.

The BD-SRDLs detected and stored more than 100 5-s-glides per day. About ten 5-s-glides (11.1 ± 5.3) were transmitted per day, along with their calculated body density values and corresponding glide parameters (Figure 4a,b; Figure S4). The transmitted and archived data were obtained for the entire migration, except for one tag (Seal ID: Prototype-1_20006) that stopped transmission mid-way due to a malfunction (Figure S4). Both transmitted and archival values of body density showed the expected trend of lipid store accumulation, where body density briefly increased, then decreased as migration progressed (Figure 4a; Figure S4). Daily body density values showed a clear one-to-one relationship between transmitted and post-processed results from the archived data (Figure 5a, $r^2=0.76$). Larger errors were observed with two seals carrying Prototype-1 BD-SRDLs with a shallower pitch threshold of 30 degrees (Figures S5 and S6). The two seals with Prototype-1 tags reached neutral buoyancy (at the drifting depth) in the middle of 7-month migrations (75–150 days after departure), characterized by the abrupt transition from −0.1 ~ +0.1 of drift rate (Figure 4c; Figure S7), determined from drift dives as reported in the previous study (Robinson et al., 2010). This transition was also reflected in increased glides occurring in the ascent phases of dives. The proportion of 5-s-glides during the ascent phase increased significantly as migration progressed and body density decreased (Figure 4d; Figure S8). This pattern in the proportion of descent/ascent 5-s-glides held for both transmitted and archived data (Figure S9).

This was also the case when we simulated the onboard algorithm on archival data on free-ranging southern elephant seals ($n=9$; dataset 2), where we detected 239,056 5-s-glides in total (Table 1). Body density values decreased as migration progressed, consistent with the expected accumulation of lipid during foraging (Figures

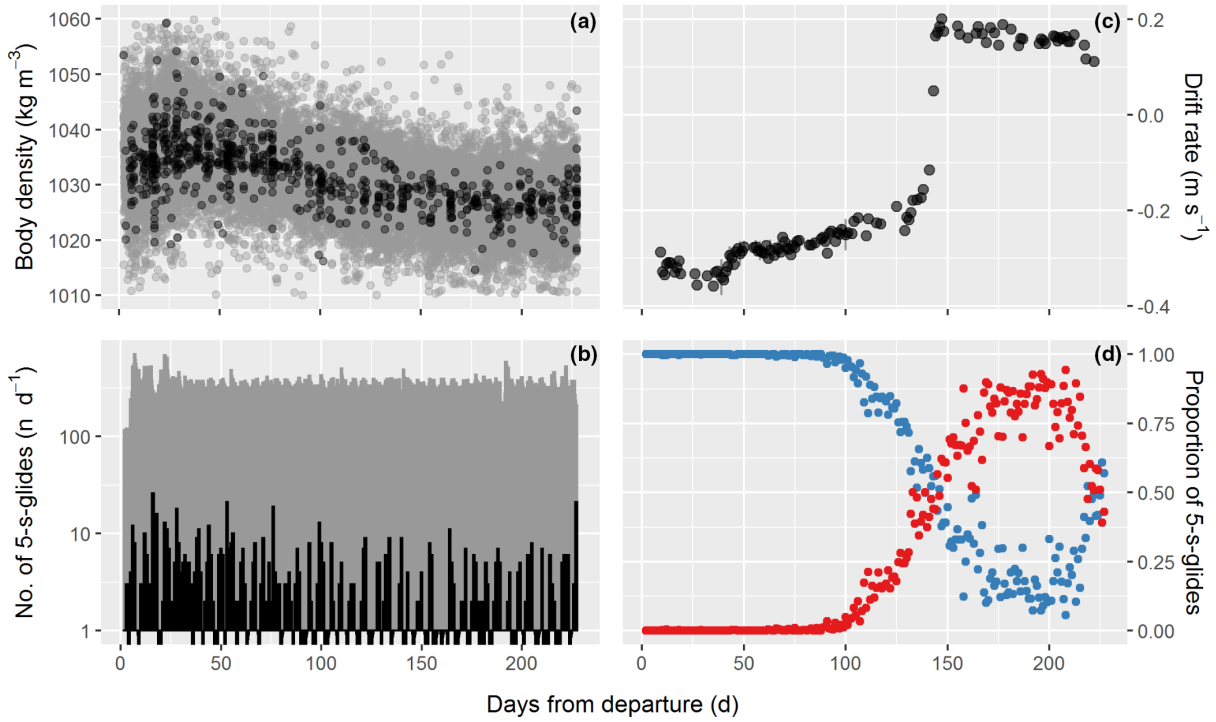

FIGURE 4 Time-series example of the Seal ID: Prototype-1_20007 during 7-month migration. (a, b) Transmitted (black) and archived (grey) body density values per 5-s-glide and daily number of 5-s-glides. Time-series data from all other seals are available in Figure S4. (c) Daily values of drift rate. Daily means ± SD are shown. (d) Daily proportion of 5-s-glides during descent versus ascent. The daily sum of descent (blue) and ascent (red) proportions is 1.0. Time-series data from all other seals are available in Figure S7 (for drift rate) and Figure S8 (for proportion of 5-s-glides).

S10A and S11). As seals became more positively buoyant, the drift rate increased (slower descent drift rate), and the descent terminal speed decreased, as expected (Figures S10A and S11). Overall, body density was negatively and positively correlated with drift rate and descent terminal speed, respectively, consistent with theoretical values (Figure S10B). The body density values estimated by the onboard algorithm showed a clear one-to-one correlation with values calculated by the desktop version of the algorithm (Figure S10B; $r^2 = 0.98$), corroborating the effectiveness of the onboard algorithm.

Overall, our onboard algorithm detected body density changes in 16 free-ranging seals as expected with respect to measured and simulated drift rate values (Figure 5b).

3.2 | Translocated seals with body density manipulation

We also simulated the onboard algorithm on archival data obtained from three translocated seals, detecting in total 3325 5-s-glides (Table 1). Body density values were higher in the weighed condition (i.e. more negatively buoyant condition), showing the negative correlation with drift rate as expected. However, the number of drift dives was limited (Figure S12A,B). This pattern agrees with the observed stroking behaviour, in which descent glides became less common, and ascent stroke amplitude became weaker right after releasing the weight (Figure S12C). The results confirmed that the changes in drifting and stroking behaviour were due to changes in the experimentally manipulated body density.

3.3 | Investigation on source of errors in body density estimation

Our body density estimation has variations in values (e.g. error bars in Figure 5a), and field tests of BD-SRDL implies that pitch threshold is key to reducing errors in body density estimation (Figure S6). To quantify the contribution of a higher pitch threshold to minimize estimation errors relative to other potential parameters, we conducted a further investigation using dataset 2 ($n = 9$, having high-sampling raw depth and three-axis acceleration archival data from free-ranging seals; Table 1) (Figure 6). Here, four potential parameters were selected as in a previous study (Aoki et al., 2011); (i) pitch angle, (ii) pitch change during the 5-s-glide, (iii) swim speed and (iv) MSE (mean square error) in a linear correlation with swim speed against time to derive the acceleration a, where larger MSE indicates weaker correlation (i.e. including more noise in the data). With this set of parameters, we conducted a sensitivity analysis to see how each parameter affected the accuracy of body density estimation as follows; (i) time-series data of measured body density values per 5-s-glide (with pitch angle > |30| degree) per seal was processed using the *gam* function in the MGCV package distributed via R (Wood, 2001) to fit a generalized additive model (GAM) with body density as a

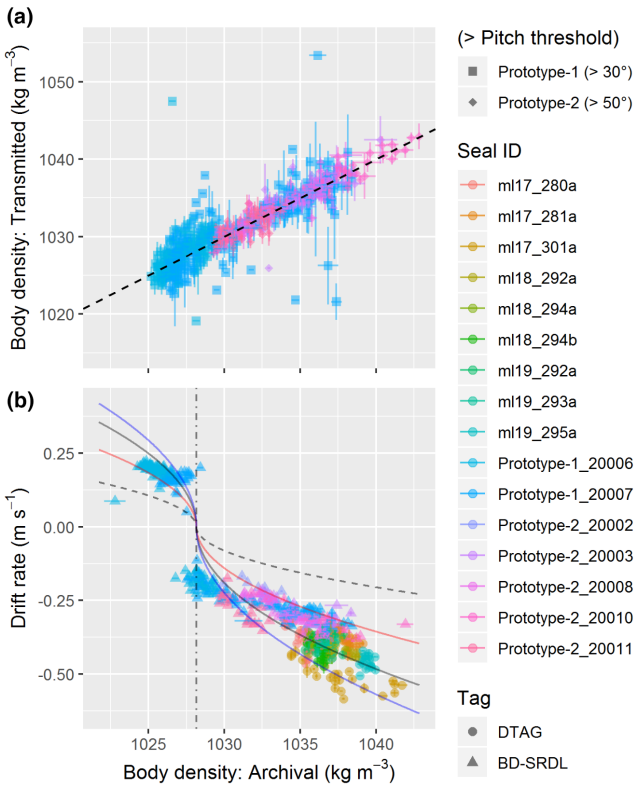

FIGURE 5 Onboard algorithm tracked the expected trend of lipid store accumulation in relation to drift rate. (a) Transmitted versus archived body density values showed a strong one-to-one correlation, validating the onboard calculation. Daily means ± SE are shown. A dotted black line represents $y=x$. Note that errors were larger in Prototype-1 with a shallower pitch threshold (30°, filled squares) than Prototype-2 (50°, filled diamonds) (see also Figure S6). (b) Body density values showed good correlation with empirical and simulated drift rates in data from DTAG (filled circles) and BD-SRDLs (filled triangles). Solid curves show simulated drift rate with $C_{d,s}=0.09$ (blue), black (0.12) and 0.23 (red), which were minimum, median and maximum estimates for $C_{d,s}$ as shown in Figure 3b. The dotted curve shows simulated drift rate with $C_{d,s}=0.69$ as per Biuw et al. (2003). Note that some data points are missing in (a) compared with (b) because transmitted data were not available for all days (see Figure 4b, Figure S4; e.g. Prototype-1_20006 stopped transmission near the middle of migration).

response variable and time as an explanatory variable. We obtained a smoothed curve of body density changes over time (Figure 6b). (ii) The measured body density values were subtracted from the fitted values to calculate the residuals for each 5-s-glide. (iii) The residuals of the 5-s-glides were squared (Figure 6b). (iv) Then, the data from all nine seals data were aggregated together (404,964 5-s-glides > |30| degree pitch). (v) The aggregated data were processed using the *gam* function to fit a generalized additive mixed model (GAMM) with squared residuals as a response variable and the set of four parameters (i.e. pitch angle, pitch change, swim speed and MSE) as explanatory variables, including individual as a random effect.

The result shows that body density errors (represented as squared residuals here) were smaller for steeper pitch angles, smaller pitch changes, lower swim speeds and smaller MSEs (Figure 6c–f). For example, when we applied median values of each parameter as thresholds (i.e. pitch angle >51.18, pitch change <3.00, swim speed <2.18 and MSE <0.07), the pitch angle threshold alone can dramatically reduce body density errors (Figure 6g).

4 | DISCUSSION

Our devices obtained empirical data that generated verified estimates of body condition of deep-diving seals. Furthermore, the tags relayed these data via the CLS Argos system in near real time.

Transmitted body density values were validated against both archival body density and drift rate values in northern elephant seals (Figure 5). While body density estimates from seals at sea have previously been demonstrated in elephant seals, the temporal and spatial resolution of such estimates have been limited because of the limited occurrence of drift dives. However, because short glides during dives are relatively frequent during foraging, the methodology developed here improves the temporal and spatial resolution to detect changes in body composition. It can also be used in other species that rarely or never exhibit drift dives. The algorithm demonstrated here should generally be applicable for deep divers that glide >100 m depth, minimizing the influence of residual gas (Biuw et al., 2003).

Further considerations below will facilitate the refinement of our onboard system for future use on other species to enhance the accuracy of body density estimation.

4.1 | Pitch angle

In daily body density estimates on field tests of the BD-SRDL, the residuals from a linear regression was larger in Prototype-1 with a shallower pitch threshold (Figure 5a; Figure S6). This implies that uncertainty in pitch angle (particularly at shallow pitch, where lift could have more effect on the hydrodynamic glide performance) can be a significant source of error when calculating body density in our method. This is reasonable because two key glide parameters in Equation (2) rely on pitch angle θ; (i) swim speed U is calculated by trigonometric function ($U=\triangle\text{Depth}/\sin\theta$), where larger θ provides more accurate estimate of swim speed because the effect of θ on $\sin\theta$ is smaller as θ becomes larger (Figure 6a) and consequently, (ii) acceleration a (i.e. slope in a linear correlation of swim speed against time) is also affected by pitch angle θ through the above swim speed calculation. Further investigation of archival high-sampling data (dataset 2) confirmed that a higher pitch angle was essential for accurately estimating body density (Figure 6g).

Although our results do not provide any specific value of an 'optimal' pitch threshold for future application of our method, we suggest using the highest pitch angle glides as this should enhance the accuracy of body density estimation. One practical strategy to make

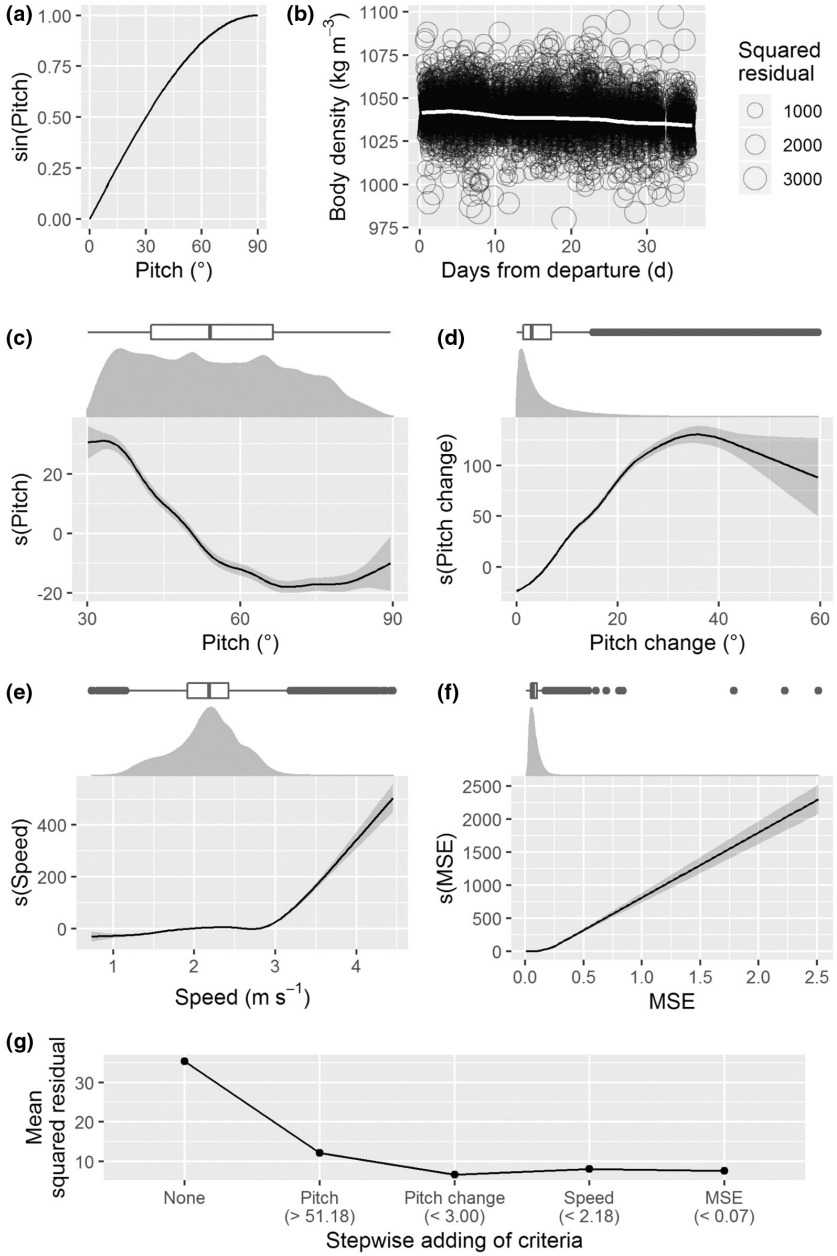

FIGURE 6 Pitch angle θ during 5-s-glides affected the consistency of the body density calculation. (a) Pitch angle θ plotted against sinθ, showing that the effect of θ on sinθ is smaller as θ becomes larger (i.e. steeper angles). (b) Time-series example of archival body density values per 5-s-glide (Seal ID: ml17_301a). The size of black spheres indicates squared residuals from the smoothed curve (white) obtained from a generalized additive model (GAM). (c–f) The results of generalized additive mixed model (GAMM), showing that body density errors become smaller with steeper pitch angle (c), smaller pitch change (d), slower swim speed (e) and lower MSE (mean square error; f) in the linear correlation of swim speed against time to calculate acceleration *a*. (g) Stepwise adding criteria show how each parameter affected variability of body density estimates. When we applied the median values of each parameter as thresholds (i.e. pitch angle >51.18, pitch change <3.00, swim speed <2.18, and MSE < 0.07; see panels c–f), the pitch angle threshold (i.e. >51.18) alone effectively reduced residuals in body density estimates, confirming that pitch angle threshold is key to reduce noise in body density estimation. Means ± SE are shown, but SE is relatively small enough not to be visible in the plot (SEs = 0.17, 0.08, 0.06, 0.12, and 0.11 for None, Pitch, Pitch change, Speed and MSE, respectively).

our method more applicable to other species is to implement a new onboard program that prioritizes 5-s-glides with higher pitch angles to send via satellite. This simple onboard selection should reduce body density errors because pitch angle mathematically governs swim speed and acceleration calculation in any species.

4.2 | Residual air in shallow divers

Additional steps would be needed to apply our method to shallower divers in terms of depth threshold to detect glides (e.g. humpback whales: Narazaki et al., 2018). The current method sets 100 m depth as the threshold to minimize the effect of lung air on body density estimation, a simplification for deep-diving animals. However, such deep-depth thresholds may not apply to other shallow-diving animals that infrequently reach 100 m depths. For future applications of our method on shallower diving animals, it is essential to consider the effect of lung air in Equation (2), as in Miller et al. (2016). Such a future implementation, accounting for gas effects on buoyancy, would make our method potentially applicable to most breath-hold divers.

4.3 | Drag coefficient

A key component in our transmission schedule is that the tag sends not only the derived value of body density (ρ_{seal}) but also glide parameters (a, ρ_{sw}, U, and θ) in Equation (2) via satellite (Figure 2b). This design helps to deal with the uncertainty of the value of the gliding drag coefficient $C_{d,f}$. In fact, although we empirically found the best-fit value of $C_{d,f}$ for our study animals, we also found that the

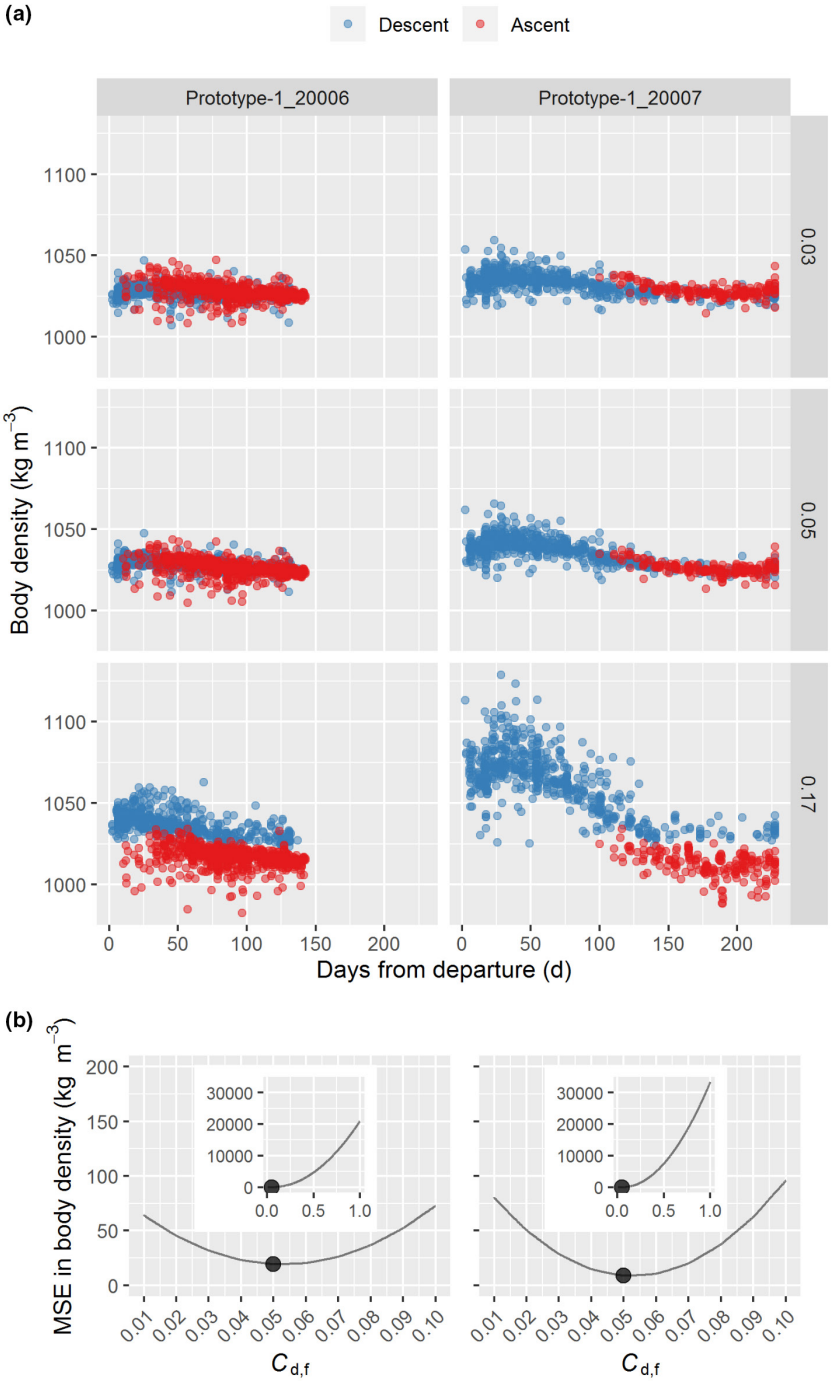

FIGURE 7 Post-hoc body density calculation is possible with transmitted glide parameters to deal with uncertainty of $C_{d,f}$. Examples are shown of two free-ranging northern elephant seals during 7-month migrations (Left: Prototype-1_20006; Right: Prototype-1_20007). (a) Seals experienced large body density changes and conducted both descent (blue) and (red) ascent 5-s-glides. The $C_{d,f}$ values of 0.03 (top panels in (a)) and 0.17 (bottom panels in (a)) are from our analysis in Figure 3a and a previous study (Aoki et al., 2011), respectively The difference in body density from descent and ascent 5-s-glides appears minimized for $C_{d,f}=0.05$ (middle), (b) which is confirmed by calculating mean squared errors (MSE) against $C_{d,f}$ values (from 0.01 to 1, by 0.01 increments). MSE was calculated between daily body density values obtained from descent and ascent 5-s-glides.

$C_{d,f}$ values reported in the literature can vary, even in the same species. This highlights the importance of transmitting glide parameters, because this enables post-hoc estimation of body density with the updated value of the $C_{d,f}$.

The $C_{d,f}$ could be obtained from the transmitted data by exploring body density values calculated from descent and ascent 5-s-glides. For example, in Prototype-1 BD-SRDL, transmitted data included descent and ascent 5-s-glide because the seals, during the long 7-month migration, experienced large body density changes and reached neutral buoyancy (Figure 4a,c; Figure S7). As a seal's body density does not change much within a day, Equation (2) can be used for both descent and ascent glides reflected in the sign of pitch (θ), and should derive identical (or similar) body density values per day. We calculated MSEs between daily body density values by descent and ascent 5-s-glides and found that $C_{d,f}$ values affected body density estimates in descent verses ascent 5-s-glides, and the difference was minimized by setting $C_{d,f}=0.05$ for both seals (Figure 7). $C_{d,f}=0.05$ is within the range of estimated $C_{d,f}$ values based on descent prolonged glides as shown in Figure 3a. This suggests that this method of post-hoc estimation of $C_{d,f}$ and body density could be effective and useful, particularly in situations where the BD-SRDL is applied on the species, for which the $C_{d,f}$ value is unknown. In this case, a $C_{d,f}$ could be obtained after the deployment. Thus, we advocate that it is essential to transmit glide

parameters (a, ρ_{sw}, U and θ) using our method to increase applicability to new species.

4.4 | Species-specific considerations

Finally, we recommend a set of practical considerations that should be carried out for future applications of our method with new species. A primary consideration is the availability of an effect tag attachment method to enable tracking of body condition changes over long-term deployments. In cetacean studies, long-duration tagging is challenging using a suction-cup method, the standard non-harmful protocol, to minimize the effect on the tagged animals. Invasive tags can function over long durations, but remotely deployed tags cannot be precisely oriented on the animal as is possible with temporarily captured seals. Thus, the use of this method entails practical limitations, and further refinements would be required to maximize the potential of the usage of our method. It is essential to adjust the best attachment location that enables satellite transmission in any species. The effect of the tag on hydrodynamic glide performance (e.g. effect on the frontal surface area, especially in small pinnipeds, including juveniles with relatively small heads) could be minimized by reducing the size of the battery. This could be achieved by reducing power consumption by duty-cycling onboard data processing or technological advances in greater battery energy density.

Preliminary field tests to collect archival time-series data of high-rate depth and acceleration data would enable species-specific adjustments of our method for fine-tuning pitch angle corrections, pitch angle thresholds, depth thresholds and potential modifications to the biomechanical model by adding new parameters such as the effect of the lung air volume or lift. The 100 m depth threshold specified here (with an exhale diver) might need to be refined for species that dive on inhalation and thereby dive with a greater volume of gas. Such preliminary data collection and analysis would maximize the potential benefits of our method with new species.

5 | CONCLUSIONS

The novel BD-SRDL enabled real-time monitoring of body condition changes at sea for over 200 days in deep-diving elephant seals. An essential component of our method is transmitting glide parameters, which enables post-hoc estimation of body density in the case where the gliding drag coefficient is unknown prior to tag deployment. Future implementation of the effect of lung air at shallow depth and species-specific considerations of tag attachment will make our method potentially applicable to any diving animal. Because the tags perform the complex data processing on board, they allow us to monitor the trajectory of animals' resource acquisition while simultaneously obtaining measures of behavioural and environmental parameters. This is possible because they require only modest energy and transmission bandwidth. We hope this methodology will facilitate the transition from indirectly inferring foraging success from behavioural shifts to directly monitoring their body condition relative to feeding effort, habitat, ecological factors and anthropogenic disturbances in the changing ocean. Furthermore, the success demonstrated here might encourage the application of using a modification of such approaches on other diving animals. While buoyancy provides a straightforward approach in the aquatic realm, analysis of acceleration signals combined with other parameters may provide relative measures of foraging success, even in flying and running animals.

AUTHOR CONTRIBUTIONS

Patrick J. O. Miller conceived the study. James Turnbull and Philip Lovell developed tags and on-board algorithms with input from Taiki Adachi, Mike A. Fedak and Patrick J. O. Miller, and authored supplementary file 1 describing the technical methods to implement the tags. All authors participated in data collection. Taiki Adachi conducted the analysis with input from Philip Lovell, Mike A. Fedak, Martin Biuw and Patrick J. O. Miller. Taiki Adachi, Mike A. Fedak and Patrick J. O. Miller wrote the manuscript with input from all co-authors.

ACKNOWLEDGEMENTS

We thank the Costa Lab members, Crocker Lab members, the field assistants at the University of California, Santa Cruz (UCSC), and the rangers and docents at Año Nuevo State Park for invaluable support during fieldwork on northern elephant seals. We thank Dr. S. J. Trumble, Dr. S. Kanatous and their laboratory members for their assistance with the translocation experiments and Mark Johnson for providing DTAG data. This study was supported by grants from the Office of Naval Research N00014-18-1-2822, DoD SERDP contract W912HQ20C0056, IPEV (Institut Paul Emile Victor) under the Antarctic research program 109 (C. Barbraud) and 1201 (C. Gilbert & C. Guinet), and CNES-TOSCA as part of the SNO-MEMO.

CONFLICT OF INTEREST STATEMENT

The authors declare no competing interest.

PEER REVIEW

The peer review history for this article is available at https://www.webofscience.com/api/gateway/wos/peer-review/10.1111/2041-210X.14089.

DATA AVAILABILITY STATEMENT

Data available via the Dryad Digital Repository https://doi.org/10.7291/D1R38H (Adachi et al., 2023).

ORCID

Taiki Adachi https://orcid.org/0000-0001-8395-4245
Mike A. Fedak https://orcid.org/0000-0002-9569-1128
Christophe Guinet https://orcid.org/0000-0003-2481-6947
Theresa R. Keates https://orcid.org/0000-0002-4833-323X
Rachel R. Holser https://orcid.org/0000-0002-8668-3839
Daniel P. Costa https://orcid.org/0000-0002-0233-5782
Patrick J. O. Miller https://orcid.org/0000-0001-8028-9673

REFERENCES

Adachi, T., Costa, D. P., Robinson, P. W., Peterson, S. H., Yamamichi, M., Naito, Y., & Takahashi, A. (2017). Searching for prey in a three-dimensional environment: Hierarchical movements enhance foraging success in northern elephant seals. *Functional Ecology*, *31*(2), 361–369. https://doi.org/10.1111/1365-2435.12686

Adachi, T., Lovell, P., Turnbull, J., Fedak, M. A., Picard, B., Guinet, C., Biuw, M., Keates, T. R., Holser, R. R., Costa, D. P., Crocker, D. E., & Miller, P. J. O. (2023). Data from: Body condition changes at sea: Onboard calculation and telemetry of body density in diving animals. *Dryad Digital Repository*, https://doi.org/10.7291/D1R38H

Adachi, T., Maresh, J. L., Robinson, P. W., Peterson, S. H., Costa, D. P., Naito, Y., Watanabe, Y. Y., & Takahashi, A. (2014). The foraging benefits of being fat in a highly migratory marine mammal. *Proceedings of the Royal Society B: Biological Sciences*, *281*(1797), 20142120.

Adachi, T., Takahashi, A., Costa, D. P., Robinson, P. W., Hückstädt, L. A., Peterson, S. H., Holser, R. R., Beltran, R. S., Keates, T. R., & Naito, Y. (2021). Forced into an ecological corner: Round-the-clock deep foraging on small prey by elephant seals. *Science Advances*, *7*(20), eabg3628. https://doi.org/10.1126/sciadv.abg3628

Andersen, J. M., Stenson, G. B., Skern-Maurizen, M., Wiersma, Y. F., Rosing-Asvid, A., Hammill, M. O., & Boehme, L. (2014). Drift diving by hooded seals (*Cystophora cristata*) in the Northwest Atlantic Ocean. *PLoS ONE*, *9*(7), e103072.

Aoki, K., Isojunno, S., Bellot, C., Iwata, T., Kershaw, J., Akiyama, Y., Martín López, L. M., Ramp, C., Biuw, M., Swift, R., Wensveen, P. J., Pomeroy, P., Narazaki, T., Hall, A., Sato, K., & Miller, P. J. O. (2021). Aerial photogrammetry and tag-derived tissue density reveal patterns of lipid-store body condition of humpback whales on their feeding grounds. *Proceedings of the Royal Society B: Biological Sciences*, *288*(1943), 20202307.

Aoki, K., Watanabe, Y. Y., Crocker, D. E., Robinson, P. W., Biuw, M., Costa, D. P., Miyazaki, N., Fedak, M. A., & Miller, P. J. O. (2011). Northern elephant seals adjust gliding and stroking patterns with changes in buoyancy: Validation of at-sea metrics of body density. *Journal of Experimental Biology*, *214*(17), 2973–2987.

Arce, F., Bestley, S., Hindell, M. A., McMahon, C. R., & Wotherspoon, S. (2019). A quantitative, hierarchical approach for detecting drift dives and tracking buoyancy changes in southern elephant seals. *Scientific Reports*, *9*(1), 8936.

Arnbom, T., Fedak, M. A., & Boyd, I. L. (1997). Factors affecting maternal expenditure in southern elephant seals during lactation. *Ecology*, *78*(2), 471–483. https://doi.org/10.2307/2266023

Bailleul, F., Charrassin, J.-B., Ezraty, R., Girard-Ardhuin, F., McMahon, C. R., Field, I. C., & Guinet, C. (2007). Southern elephant seals from Kerguelen Islands confronted by Antarctic Sea ice. Changes in movements and in diving behaviour. *Deep-Sea Research Part II: Topical Studies in Oceanography*, *54*(3–4), 343–355.

Beltran, R. S., Kendall-Bar, J. M., Pirotta, E., Adachi, T., Naito, Y., Takahashi, A., Cremers, J., Robinson, P. W., Crocker, D. E., & Costa, D. P. (2021). Lightscapes of fear: How mesopredators balance starvation and predation in the open ocean. *Science Advances*, *7*(12), eabd9818.

Biuw, M., Boehme, L., Guinet, C., Hindell, M., Costa, D., Charrassin, J.-B., Roquet, F., Bailleul, F., Meredith, M., Thorpe, S., Tremblay, Y., McDonald, B., Park, Y.-H., Rintoul, S. R., Bindoff, N., Goebel, M., Crocker, D., Lovell, P., Nicholson, J., … Fedak, M. A. (2007). Variations in behavior and condition of a Southern Ocean top predator in relation to *in situ* oceanographic conditions. *Proceedings of the National Academy of Sciences of the United States of America*, *104*(34), 13705–13710.

Biuw, M., McConnel, B., Bradshaw, C. J. A., Burton, H., & Fedak, M. (2003). Blubber and buoyancy: Monitoring the body condition of free-ranging seals using simple dive characteristics. *Journal of Experimental Biology*, *206*(19), 3405–3423. https://doi.org/10.1242/jeb.00583

Boyer, T. P., Baranova, O. K., Coleman, C., Garcia, H. E., Grodsky, A., Locarnini, R. A., Mishonov, A. V., Paver, C. R., Reagan, J. R., Seidov, D., Smolyar, I. V., Weathers, K., & Zweng, M. M. (2018). World Ocean Database 2018. *A.V. Mishonov, Technical Ed., NOAA Atlas NESDIS 87*.

Costa, D. P., Breed, G. A., & Robinson, P. W. (2012). New insights into pelagic migrations: Implications for ecology and conservation. *Annual Review of Ecology, Evolution, and Systematics*, *43*, 73–96.

Costa, D. P., Schwarz, L., Robinson, P., Schick, R. S., Morris, P. A., Condit, R., Crocker, D. E., & Kilpatrick, A. M. (2016). A bioenergetics approach to understanding the population consequences of disturbance: Elephant seals as a model system. In A. N. Popper & A. Hawkins (Eds.), *The effects of noise on aquatic life II. Advances in experimental medicine and biology* (Vol. *875*, pp. 161–169). Springer.

Crocker, D. E., Le Boeuf, B. J., & Costa, D. P. (1997). Drift diving in female northern elephant seals: Implications for food processing. *Canadian Journal of Zoology*, *75*(1), 27–39. https://doi.org/10.1139/z97-004

Fedak, M. A. (2013). The impact of animal platforms on polar ocean observation. *Deep-Sea Research Part II: Topical Studies in Oceanography*, *88–89*, 7–13.

Fedak, M. A., Arnbom, T., & Boyd, I. L. (1996). The relation between the size of southern elephant seal mothers, the growth of their pups, and the use of maternal energy, fat, and protein during lactation. *Physiological Zoology*, *69*(4), 887–911.

Fedak, M. A., Lovell, P., & Grant, S. M. (2001). Two approaches to compressing and interpreting time-depth information as collected by time-depth recorders and satellite-linked data recorders. *Marine Mammal Science*, *17*(1), 94–110.

Fedak, M. A., Wilson, B., & Pomeroy, P. P. (2009). Reproductive behavior. In W. F. Perrin, B. Würsig, & J. G. M. Thewissen (Eds.), *Encyclopedia of marine mammals* (pp. 943–955). Academic Press.

Fleishman, E., Costa, D. P., Harwood, J., Kraus, S., Moretti, D., New, L. F., Schick, R. S., Schwarz, L. K., Simmons, S. E., Thomas, L., & Wells, R. S. (2016). Monitoring population-level responses of marine mammals to human activities. *Marine Mammal Science*, *32*(3), 1004–1021. https://doi.org/10.1111/mms.12310

Goulet, P., Guinet, C., Campagna, C., Campagna, J., Tyack, P. L., & Johnson, M. (2020). Flash and grab: Deep-diving southern elephant seals trigger anti-predator flashes in bioluminescent prey. *Journal of Experimental Biology*, *223*, jeb222810.

Goulet, P., Guinet, C., Swift, R., Madsen, P. T., & Johnson, M. (2019). A miniature biomimetic sonar and movement tag to study the biotic environment and predator-prey interactions in aquatic animals. *Deep-Sea Research Part I: Oceanographic Research Papers*, *148*, 1–11.

Guinet, C., Vacquié-Garcia, J., Picard, B., Bessigneul, G., Lebras, Y., Dragon, A. C., Viviant, M., Arnould, J. P. Y., & Bailleul, F. (2014). Southern elephant seal foraging success in relation to temperature and light conditions: Insight into prey distribution. *Marine Ecology Progress Series*, *499*, 285–301.

Hussey, N. E., Kessel, S. T., Aarestrup, K., Cooke, S. J., Cowley, P. D., Fisk, A. T., Harcourt, R. G., Holland, K. N., Iverson, S. J., Kocik, J. F., Mills Flemming, J. E., & Whoriskey, F. G. (2015). Aquatic animal telemetry: A panoramic window into the underwater world. *Science*, *348*(6240), 1255642.

Johnson, M. P., & Tyack, P. L. (2003). A digital acoustic recording tag for measuring the response of wild marine mammals to sound. *IEEE Journal of Oceanic Engenering*, *28*(1), 3–12.

Keen, K. A., Beltran, R. S., Pirotta, E., & Costa, D. P. (2021). Emerging themes in Population Consequences of Disturbance models. *Proceedings of the Royal Society B: Biological Sciences*, *288*(1957), 20210325. https://doi.org/10.1098/rspb.2021.0325

Lumley, T. (2013). *biglm: Bounded memory linear and generalized linear models*. R package version 0.9-1.

McMahon, C. R., Burton, H., Mclean, S., Slip, D., & Bester, M. (2000). Field immobilisation of southern elephant seals with intravenous tiletamine and zolazepam. *Veterinary Record*, *146*(25), 251–254. https://doi.org/10.1136/vr.146.9.251

Miller, P. J. O., Johnson, M. P., Tyack, P. L., & Terray, E. A. (2004). Swimming gaits, passive drag and buoyancy of diving sperm whales *Physeter macrocephalus*. *Journal of Experimental Biology*, *207*(11), 1953–1967.

Miller, P., Narazaki, T., Isojunno, S., Aoki, K., Smout, S., & Sato, K. (2016). Body density and diving gas volume of the northern bottlenose whale (*Hyperoodon ampullatus*). *Journal of Experimental Biology*, *219*(16), 2458–2468.

Mitani, Y., Andrews, R. D., Sato, K., Kato, A., Naito, Y., & Costa, D. P. (2010). Three-dimensional resting behaviour of northern elephant seals: Drifting like a falling leaf. *Biology Letters*, *6*(2), 163–166.

Naito, Y., Costa, D. P., Adachi, T., Robinson, P. W., Fowler, M., & Takahashi, A. (2013). Unravelling the mysteries of a mesopelagic diet: A large apex predator specializes on small prey. *Functional Ecology*, *27*(3), 710–717.

Narazaki, T., Isojunno, S., Nowacek, D. P., Swift, R., Friedlaender, A. S., Ramp, C., Smout, S., Aoki, K., Deecke, V. B., Sato, K., & Miller, P. J. O. (2018). Body density of humpback whales (*Megaptera novaengliae*) in feeding aggregations estimated from hydrodynamic gliding performance. *PLoS ONE*, *13*(7), e0200287.

National Academies of Sciences Engineering and Medicine. (2017). *Approaches to understanding the cumulative effects of stressors on marine mammals*. The National Academies Press.

Page, B., McKenzie, J., Hindell, M. A., & Goldsworthy, S. D. (2005). Drift dives by male New Zealand fur seals (*Arctocephalus forsteri*). *Canadian Journal of Zoology*, *83*, 293–300. https://doi.org/10.1139/z05-013

Pirotta, E., Booth, C. G., Costa, D. P., Fleishman, E., Kraus, S. D., Lusseau, D., Moretti, D., New, L. F., Schick, R. S., Schwarz, L. K., Simmons, S. E., Thomas, L., Tyack, P. L., Weise, M. J., Wells, R. S., & Harwood, J. (2018). Understanding the population consequences of disturbance. *Ecology and Evolution*, *8*(19), 9934–9946. https://doi.org/10.1002/ece3.4458

Pirotta, E., Schwarz, L. K., Costa, D. P., Robinson, P. W., & New, L. (2019). Modeling the functional link between movement, feeding activity, and condition in a marine predator. *Behavioral Ecology*, *30*(2), 434–445.

Pomeroy, P. P., Fedak, M. A., Rothery, P., & Anderson, S. (1999). Consequences of maternal size for reproductive expenditure and pupping success of grey seals at North Rona, Scotland. *Journal of Animal Ecology*, *68*(2), 235–253.

Richard, G., Vacquié-Garcia, J., Jouma'a, J., Picard, B., Génin, A., Arnould, J. P. Y., Bailleul, F., & Guinet, C. (2014). Variation in body condition during the post-moult foraging trip of southern elephant seals and its consequences on diving behaviour. *Journal of Experimental Biology*, *217*(14), 2609–2619.

Robinson, P. W., Costa, D. P., Crocker, D. E., Gallo-Reynoso, J. P., Champagne, C. D., Fowler, M. A., Goetsch, C., Goetz, K. T., Hassrick, J. L., Hückstädt, L. A., Kuhn, C. E., Maresh, J. L., Maxwell, S. M., McDonald, B. I., Peterson, S. H., Simmons, S. E., Teutschel, N. M., Villegas-Amtmann, S., & Yoda, K. (2012). Foraging behavior and success of a mesopelagic predator in the northeast Pacific Ocean: Insights from a data-rich species, the northern elephant seal. *PLoS ONE*, *7*(5), e36728. https://doi.org/10.1371/journal.pone.0036728

Robinson, P. W., Simmons, S. E., Crocker, D. E., & Costa, D. P. (2010). Measurements of foraging success in a highly pelagic marine predator, the northern elephant seal. *Journal of Animal Ecology*, *79*(6), 1146–1156.

Sato, K., Watanuki, Y., Takahashi, A., Miller, P. J. O., Tanaka, H., Kawabe, R., Ponganis, P. J., Handrich, Y., Akamatsu, T., Watanabe, Y., Mitani, Y., Costa, D. P., Bost, C. A., Aoki, K., Amano, M., Trathan, P., Shapiro, A., & Naito, Y. (2007). Stroke frequency, but not swimming speed, is related to body size in free-ranging seabirds, pinnipeds and cetaceans. *Proceedings of the Royal Society B: Biological Sciences*, *274*(1609), 471–477.

Schick, R. S., Kraus, S. D., Rolland, R. M., Knowlton, A. R., Hamilton, P. K., Pettis, H. M., Kenney, R. D., & Clark, J. S. (2013). Using hierarchical Bayes to understand movement, health, and survival in the endangered North Atlantic right whale. *PLoS ONE*, *8*(6), e64166.

Watanabe, Y., Baranov, E. A., Sato, K., Naito, Y., & Miyazaki, N. (2006). Body density affects stroke patterns in Baikal seals. *Journal of Experimental Biology*, *209*(17), 3269–3280. https://doi.org/10.1242/jeb.02402

Watanabe, Y. Y., Baranov, E. A., & Miyazaki, N. (2015). Drift dives and prolonged surfacing periods in Baikal seals: Resting strategies in open waters? *Journal of Experimental Biology*, *218*(17), 2793–2798.

Williams, T. M., Davis, R. W., Fuiman, L. A., Francis, J., Le Boeuf, B. J., Horning, M., Calambokidis, J., & Croll, D. A. (2000). Sink or swim: Strategies for cost-efficient diving by marine mammals. *Science*, *288*(5463), 133–136. https://doi.org/10.1126/science.288.5463.133

Wood, S. N. (2001). mgcv: GAMs and generalized ridge regression for R. *R News*, *1*(2), 20–25.

SUPPORTING INFORMATION

Additional supporting information can be found online in the Supporting Information section at the end of this article.

Data S1: Technical description of the methods used to implement the BD-SRDL tag.**Data S2:** Supplementary Figures.

How to cite this article: Adachi, T., Lovell, P., Turnbull, J., Fedak, M. A., Picard, B., Guinet, C., Biuw, M., Keates, T. R., Holser, R. R., Costa, D. P., Crocker, D. E., & Miller, P. J. O. (2023). Body condition changes at sea: Onboard calculation and telemetry of body density in diving animals. *Methods in Ecology and Evolution*, *00*, 1–18. https://doi.org/10.1111/2041-210X.14089